Applied Surface Science 614 (2023) 156204

Contents lists available at ScienceDirect

Applied Surface Science

journal homepage: www.elsevier.com/locate/apsusc

Full Length Article

Interaction mechanism of transition metal phthalocyanines on transition metal nitride supports

Philip Mantos [a,b,1], Chase Ferrone [a,1], Taisuke Ohta [c], Pabitra Choudhury [a,*], Sanchari Chowdhury [a,*]

[a] Department of Chemical Engineering, New Mexico Tech, NM 87801, USA
[b] Department of Materials and Metallurgical Engineering, New Mexico Tech, NM 87801, USA
[c] Sandia National Laboratories, Albuquerque, NM 87185, USA

ARTICLE INFO

Keywords:
Electronic interaction
Work function
Transition metal nitride
Transition metal phthalocyanine
Density functional theory
Photoelectron emission microscopy

ABSTRACT

We investigated the electronic interactions between transition metal phthalocyanine (TMPc's) on a refractory transition metal nitride support, specifically copper phthalocyanine (CuPc) on titanium nitride (TiN). X-ray Photoelectron Spectroscopy (XPS) results suggest a presence of a few nanometer native oxide layer on the surface of the TiN nanoparticles, which consists of TiN, TiO_2, and Titanium oxynitrides ($Ti_xO_yN_z$). A TiNCuPc nanocomposite was synthesized via a simple mixing method due to the strong binding between CuPc and TiN confirmed by density functional theory (DFT) calculations. Both XPS data and DFT calculations revealed an electron transfer from TiN substrate to CuPc molecule. The nature of charge transfer is not influenced by the presence of an oxide layer on the surface of TiN. Substantial deviations are however found between photoelectron emission microscopy (PEEM) measured work function for TiN (4.68 eV) and theoretically calculated work function for pristine stoichiometric TiN (2.63 eV). This behavior is attributed to the presence of an oxide layer on the TiN surface. TiNCuPc composite system has a work function value between those of TiN and CuPc. Our studies open up an opportunity to apply a new class of materials based on transition metal phthalocyanine/transition metal nitride composites to catalysis and optoelectronic devices.

1. Introduction

Transition metal phthalocyanines are an interesting class of organic semiconductors due to their high catalytic activity, photostability, stability against harsh conditions and tunable properties. Their properties can be easily and selectively tailored by changing the transition metal center. These materials have wide range of applications including optoelectronic devices, field-effect transistors, and organic photovoltaics as well as for catalysis.[1] Transition-metal phthalocyanine (TMPc) gains increasing attentions as important electrocatalysts for oxygen reduction reaction (ORR).[2] Additionally, TMPc materials have suggested usage as bioinspired catalysts for C—H bond breaking reactions.[3] The efficiency of TMPc based materials as catalysts highly depends on the interaction processes at the interface between these organic material and the substrate. In particular electronic properties and the interfacial local charge transfer between the transition metal of the TMPc and substrates are significantly influenced by the nature of the substrates.[4] For instance, for TMPc, a strong charge transfer interaction is observed at the interface with gold, silver, nickel, or graphene.[5–7] Here, we studied copper phthalocyanine (CuPc) on a long-term stable refractory transition metal nitride supports, titanium nitride (TiN). Copper phthalocyanine is known as a stable and active catalyst with different applications in fuel cells[2], direct oxidation cells [3], and wastewater treatment[4]. Refractory transition metal nitrides such as titanium nitride are an attractive catalytic support due to their stability at high temperatures as well as in harsh chemical conditions. TiN has also been identified as a promising candidate for catalyst support to be used in many different electrochemical, thermal reactions as well as photocatalytic reactions for many different metal catalysts including Ni, Pd, and Pt.[6–10].

TiN nanomaterials are an attractive option as a noble metal-free catalysts as well as catalytic support materials for fuel cell and different reactions including electrodeposition, methanol oxidation reaction, ethanol oxidation reaction, formic acid oxidation reaction, and

* Corresponding authors.
E-mail addresses: pabitra.choudhury@nmt.edu (P. Choudhury), sanchari.chowdhury@nmt.edu (S. Chowdhury).
[1] Authors have equal contribution.

https://doi.org/10.1016/j.apsusc.2022.156204
Received 12 October 2022; Received in revised form 30 November 2022; Accepted 20 December 2022
Available online 22 December 2022

oxygen reduction reaction. [11,12,13]. In addition to better stability and low cost, the performance of TiN towards oxygen reduction reactions is comparable with platinum which is traditionally considered as the best catalysts for oxygen reduction reactions. In contrast, silver, and gold exhibit poor catalytic performance towards ORR due to the weak chemisorption properties caused by the filled d-band.

TiN based catalytic supports are particularly advantageous due to their strong electronic interaction with the supported metal catalysts. TiN has shown promise as a catalytic support for direct hydrogen and methanol fuel cells.[14] One of the key aspects of transition metal nitrides, such as TiN, is the wide variation of stoichiometry. For example, TiN_x can exist in a range from $\times = 0.5$ to $\times = 1$.[15] This wide range of stoichiometry presents an opportunity to alter the surface nitrogen density to directly change the number of anchoring sites on TiN.[16,17] Much attentions are paid to CuPc/TiO_2 for different applications ranging from catalytic reactions to hybrid memory element due to strong interaction between TiO_2 and CuPc.[4,10,14,15] A few nanometer native self-passivating oxide layers is present on the TiN surface, and can interact strongly with TMPc molecules. [18,19] In addition to excellent stability of titanium nitride, these materials show strong plasmonic properties under visible light offering an opportunity to use solar light to enhance any processes that involve this materials[9]. This can make TiN a better alternative than TiO_2 to support CuPc. Therefore, CuPc molecules at the TiN surface is worth studying.

Here for the first time, TiN is investigated as a supporting material for TMPc. We studied the structural and compositional properties of CuPc/TiN composites using High resolution transmission electron microscopy (HRTEM), Fourier Transform Infrared Spectroscopy (FTIR) and X-ray diffraction (XRD). We used Photoelectron Emission microscopy (PEEM) to predict how the addition of CuPc to TiN affects its work functions. The knowledge of the work functions, which in turn can give an estimate of the ionization energies, is important for the design of catalysts. In order to evaluate the charge transfer among TiN and CuPc we used X-ray photoelectron spectroscopy (XPS). The electronic properties of the TiN/CuPc composites are further confirmed using density functional theory (DFT) calculations. Our study also revealed how the presence of a native oxide layer on TiN may affect their interactions with the catalysts supported on them.

2. Material and methods:

2.1. Synthesis methods

CuPc/TiN composites were synthesized by mixing 1 mg/mL of CuPc with 1 mg/mL TiN, in 5 mL DMF. Samples were sonicated for 4 hrs while varying their position every hour to avoid high power zones inside the sonicator. DMF was chosen as a synthesis as it showed high solubility for both CuPc and TiN. After being synthesized, the CuPc/TiN composites were separated through centrifugation at 3.3 k Rcf for 90 min. Supernatants were discarded and pellets were re-dispersed in DI water. The dispersed pellets were subjected to centrifugation once again at the same operating parameters. Once sonicated, the organic phase as well as the supernatant were decanted and dried at 80 °C. The remaining pellet was dispersed in DI water for UV–vis spectroscopy, and in Isopropyl alcohol for electron microscopy, or in potassium bromide for FTIR studies.

2.2. Characterizations:

UV–vis absorbance spectra of the samples were measured using a Thermo Scientific Evo260 Ultraviolet Visible Spectrum Spectrometer across a range of 200 nm to 1100 nm. For UV–vis spectrum of liquid phase solution of the samples, the powder was dispersed in a DI water. Quartz cuvettes were used for the measurement, as glass cuvettes are absorptive in the range below 400 nm. Diffuse reflectance was also used for solid phase powdered samples. Samples were ground in potassium bromide in a 40:1 or 80:1 wt ratio depending on the optical absorbance of the sample. Diffuse reflectance was taken across the same wavelength range as above using the UV–vis.

FTIR was taken on a Nicolet Is50 FTIR using a Harrick DRP praying mantis accessory. Samples were mixed in a 40:1 or 80:1 wt ratio with potassium bromide to prevent oversaturation. FTIR data sets were recorded as the average of 32 scans at a resolution of 8 scans. Backgrounds were collected every hour at minimum to account for changes in the surrounding atmosphere.

XPS samples were prepared by drying TiNCuPc composites at 90 °C for 1 hr and being collected in a powdered form. XPS measurements were performed using a Kratos Ultra DLD spectrometer. TiN, CuPc and TiNCuPc samples were scanned, resulting in a full range scan as well as a high-resolution scan for Nitrogen, Carbon, Oxygen, Titanium, and Copper. Raw response data from the XPS were normalized via an assumption of summations between normal distributions and matched to existing libraries of binding energies. The XPS scans can give an approximation of the surface of each sample as XPS only probes about 3 nm into the sample.

The samples for PEEM study were prepared by drop casting samples onto 1 cm^2 Silicon wafers with native silicon oxide. PEEM measurements were conducted in a LEEM-III system (Elmitec Elektronenmikroskopie GmbH) with a tunable deep ultraviolet light source. Samples were exposed to ultrahigh vacuum condition and a 20 kV during the PEEM measurement. Photoemission spectra were recorded by sweeping through the kinetic energies of the photoemitted electrons (typical sweeping range ~ 5 eV) with respect to an electron energy filter.

Raw PEEM data was processed to remove effects from both an electron energy filter's dispersion which causes a change in onset position and an uneven background intensity which can add a non uniform addition of intensity in the sample if not corrected for.

In PEEM studies the collected data set were in form of 2 dimensional images recording the photoelectron intensity over an × and y range with each image being taken at a different electron kinetic energy. Each image was then compiled into a 3-dimensional data set where × and y were lateral dimensions and z was a dimension for the change in the electron kinetic energy. This allowed for any spot on the image to have its intensity tracked over a range of electron kinetic energy studied. The vacuum level and the valence band information were obtained by fitting the photoemission spectra at each pixel and by correcting for the dispersion of the electron energy filter using the SiO_2 background. The details of the PEEM measurement procedures and the data processing can be found in Sharma et al. [20] and its supplemental information.

2.3. Theoretical calculation method

Ab Initio Density Functional Theory calculations were used to find electronic properties of TiN, CuPc, TiNCuPc, TiO_2 and TiO_2CuPc systems. These calculations and analysis were done using the Vienna Ab Initio Simulation Package (VASP).[21] These simulations were carried out using spin polarized DFT with the Perdew-Burke-Ernzerhof (PBE) method of generalized gradient approximation (GGA) and a semi-empirical scheme proposed by Grimme for van der Waals interactions [22,23] and a plane-wave cutoff of 400 eV. Projector Augmented Wave (PAW) Potentials were used as descriptors when simulating atomic character.[24,25] Convergence was facilitated using Gaussian smearing at a width of 0.1 eV, electronic tolerance of 10^{-6} eV, and an ionic relaxation until residual forces on the ions were less than 0.02 eV/ Å. Simulations were conducted using a 3 × 3 × 1 Automatic *k*-point mesh for sampling the Brillouin Zone. Electronic and energetic interactions between TiN and the Phthalocyanine molecule were found using a Bader charge analysis evaluation.[25–28] The periodic supercell containing the catalytic system was 15 × 15 $Å^2$ in × and *y* directions and 24 Å in the *z* direction creating a vacuum such that periodic interactions would only occur in the × and y dimensions.

3. Results and Discussions:

3.1. Structural and compositional characterization:

TiN nanoparticles of average diameter at 20 nm were purchased from US Research Nanomaterials, Inc. Fig. 1 shows the morphology of TiN nanoparticles characterized using high-resolution transmission electron microscopy (HRTEM). TiN nanoparticles develop 1–2 nm thick self-passivating oxide layer on the surface as shown in Fig. 1(b). CuPc/TiN composites were synthesized by mixing CuPc and TiN in Dimethylformamide (DMF) solvent using sonication. The composites were separated and purified using centrifugation and drying. The TiNCuPc composites were first characterized by UV–vis spectroscopy [Fig. 2(a)] with CuPc and TiN as a control. The signature UV–vis absorption peaks of CuPc at 350 nm due to the B (Soret) band and, 625 nm and 725 nm peaks due to Q bands are present in both CuPc and TiNCuPc samples. in Fig. 2 (a)[29] TiN has broad absorption spectrum in the visible range.[8] The spectrum of TiNCuPc sample is overwhelmed by CuPc in the visible and IR ranges.[30].

The XRD data for the TiNCuPc sample is presented in Fig. 2(b), with the peak positions and corresponding spacings listed in Table 1. The spacings of 1.5, 2.1, and 2.4 Å corresponds to osbornite, a rock salt phase of TiN.[15] The peaks at 18.5° and 23.8° correspond to α and β phases of CuPc.[31] The peaks in the range from 26.5° to 33.2° are likely the indicators of a normalized spacing between TiN and CuPc with a height of about 3.4–2.7 Å. The larger d-spacing of 12.5 Å and 9.6 Å at low angle values of 7.1° and 9.2° are indicative that some CuPc may have formed aggregates. The presence of larger d-spacing in CuPc is due to the ordered but loose forms of aggregates.[30].

The FTIR data presented in Fig. 2(c) indicates the majority of TMPc peaks are due to interaction between organic molecules and only a small number of peaks could correspond to bonds involving the metal core. This result agrees well with the fact that the TMPc molecules only have one type of bond present around the metal core. The metal core of a CuPc should only be expected to directly interact with the two of the four nitrogen atoms that surround it. The TiN nanoparticles don't have any characteristic peaks in the range of the FTIR studied here. The FTIR spectrum corresponding to TiNCuPc is essentially the summation of TiN and CuPc indicating the adsorption of CuPc on TiN.

3.2. Electronic interaction among TiN and CuPc:

We performed XPS analysis to examine the surface stoichiometry of the samples as well as the interaction between TiN and CuPc in their composites. The XPS is sensitive to approximately the 3 nm thickness into the surface of a TiN sample. Fig. 3 (a & b) shows the high resolution XPS spectra of the Ti2p, and N1s core levels of the TiN nanoparticle surface, providing information about the chemical states of the atoms on the film surface. The spectra were deconvoluted into different components corresponding to different possible oxidation states. Both Ti 2p and N 1 s data show the peaks corresponding to TiN, as well as various oxidation states of Ti mainly in the forms of the Ti—O—N and TiO_2.[32] The quantitative analysis estimates that the surface of TiN is mostly in the form of TiO_2 (52 %) and TiON (38 %). This XPS analysis agrees qualitatively with HRTEM images of TiN, which show TiN form 1–2 nm native oxide layer on the surface (Fig. 1(b)). The N 1 s data of CuPc is presented in Fig. 3(c) which shows the presence of C—N and C—N bonds in CuPc,[33] and agrees with the molecular structure of CuPc. Our XPS data suggested the surface of TiN in TiNCuPc sample is also comprised mostly of TiO_2 and TiON (Figure SI6).

Cu 2*p* spectra of CuPc and TiNCuPc composites shed light on the charge transfer between CuPc and TiN. In Fig. 3(d), the peak representing Cu 2*p* of CuPc shifts towards lower binding energy by about 0.5 eV when it is deposited on TiN. As the peak position of Cu 2*p* is being pushed toward a lower binding energy it correlates with a lower relative oxidation state of the Cu cores present in CuPc. This shift suggests that there may be an electron transfer to the Cu metal center of CuPc resulting in gaining electrons, which is confirmed by DFT calculations as discussed in later sections. Fig. 3 (e) shows comparison N 1 *s* spectra for CuPc, TiNCuPc and TiN. The peak position of N 1 s in composite TiN-CuPc occurring at a higher eV in comparison to CuPc. This shows nitrogen is being brought towards a higher oxidation state indicating loss of electrons from nitrogen. On the other hand, Ti 2p peak of TiNCuPc shifts to lower binding energy [Fig. 3 (f)] which indicates the oxidation state of Ti reduced and implies the possibilities of electron transfer to Ti.

Density Functional Theory analysis of a TiN Copper Phthalocyanine system was conducted to further confirm our experimental observations. Binding energy, defined as the difference in energy between the system and the TiN substrate surface & CuPc species, $E_B = E_{TiN/CuPc} - E_{TiN} - E_{CuPc}$, was found to be about –7.69 eV. This high negative binding energy shows an energetically favorable formation of the TiNCuPc composite system. A charge analysis on TiNCuPc has shown that a pristine TiN substrate loses about $3e^-$ to the phthalocyanine molecule, which gains the same amount. The results clearly suggest that CuPc adsorbs very strongly on the TiN substrate. Optimized geometry displayed chemisorption between CuPc nitrogen atoms and titanium atoms on the TiN substrate. Bader charge analysis also clearly supports the XPS results. We have computed Bader charges of CuPc alone and the results showed that the transition metal active site has a net charge of + 1.08e. However, the Cu net charge decreased to + 0.89e when CuPc is supported by pristine TiN. These results indicate that TiN will transfer an extra 0.19e to the Cu atom of a phthalocyanine molecule. The 8 nitrogen atoms located in the copper phthalocyanine supported by titanium nitride had an average charge of + 2.91e from Bader analysis. The unsupported copper phthalocyanine nitrogen atoms had an average charge of −1e. Bader analysis has shown that titanium nitride donates charge to the nitrogen atoms present in the phthalocyanine, and the associated ligand nitrogen as shown in Fig. SI1 in the Supplementary Information.

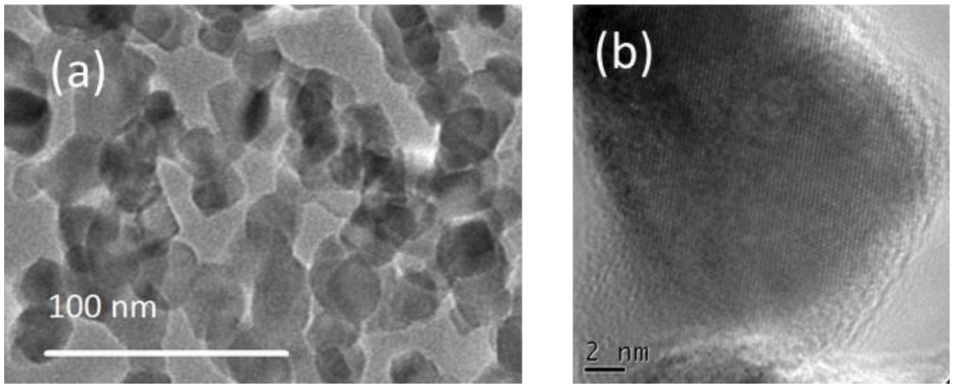

Fig. 1. (a) HRTEM of TiN nanoparticles (b) magnified image to show amorphous oxide layer on the surface of TiN nanoparticles.

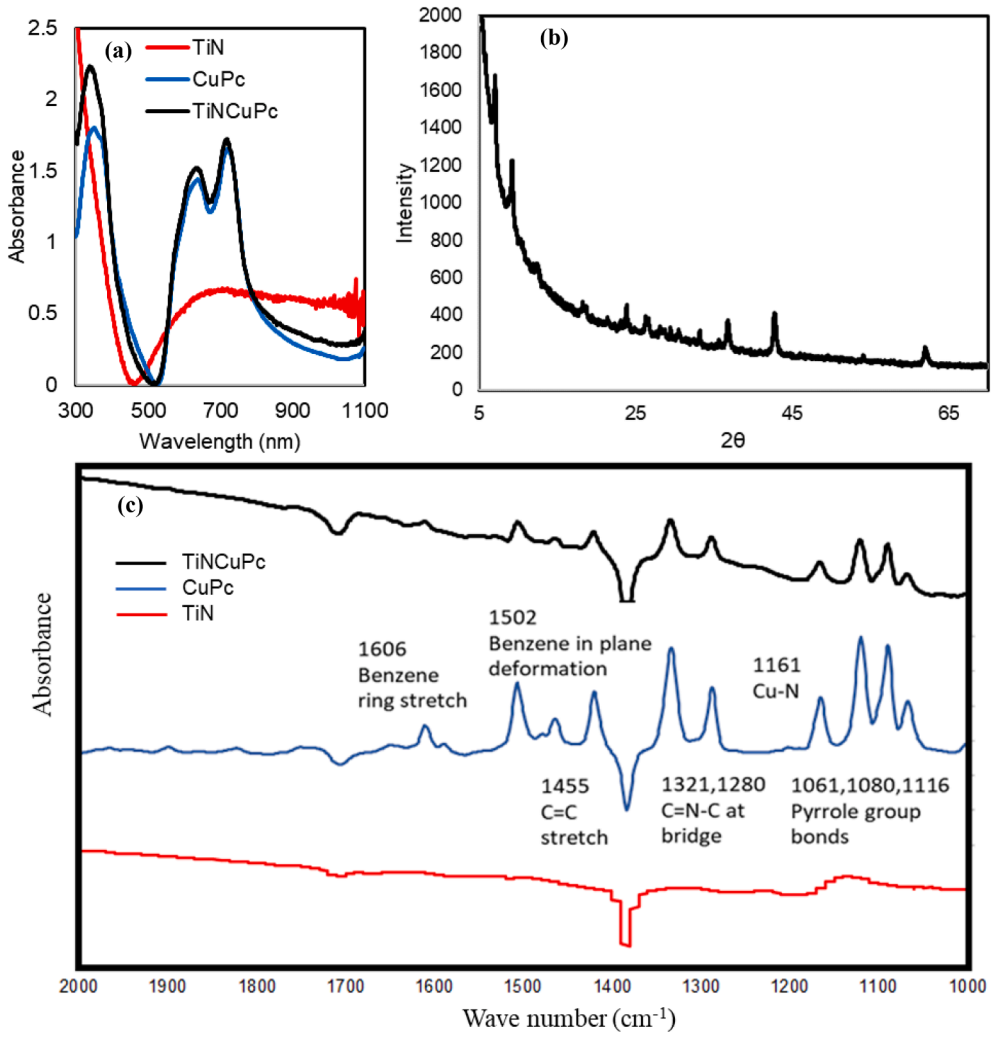

Fig. 2. (a) Diffused Reflectance UV–vis absorbance of TNCuPc composites and its constituents across the UV–Visible range. (b) XRD data of TiNCuPc composites (c) FTIR spectra of CuPc, TiN and TiNCuPc. Color should be used for (a) and (b).

Table 1
XRD peaks and corresponding spacing in TiNCuPc.

Position 2θ	7.1	9.2	18.6	23.8	26.5	33.2	36.7	42.7	61.9
Spacing A°	12.5	9.6	4.8	3.7	3.4	2.7	2.4	2.1	1.5

To account for TiN surface oxidation, a 2 % oxygen substitution in TiN and as well as a TiO_2 substrate were analyzed. In both cases, the oxidized substrates still promoted charge transfer to the CuPc molecule with copper charges of + 0.89 and + 0.80e, respectively. To support the Bader charge analysis, a charge density difference (CDD) isosurfaces of TiN/CuPc system as shown in Fig. 4(a) was also calculated. The Fig. 4(a) clearly depicts the similar electron transfer from the substrate (charge depletion shown by green isosurface) to CuPc (charge accumulation shown by yellow isosurface) for the pristine TiN/CuPc. Furthermore, the plane average CDD as shown in Fig. 4(b) displays the change in charge as a function of unit cell height where the lower positioned substrate donates charge to the CuPc.

3.3. Work functions determination through PEEM imaging and theoretical calculations

PEEM samples were prepared by drop casting CuPc, TiN, and TiNCuPc samples onto Silicon wafers with native silicon oxide. Detailed data processing protocols are given in reference [34]. Briefly, samples were imaged under high vacuum and a 20 kV acceleration voltage. A series of images were taken gathering the photoelectron intensity of each pixel in the field of view as the starting voltage of the systems range from −4 to + 3 eV. This starting voltage is used to control the kinetic energy of the electrons reaching the sample surface. These photoelectron intensity v. starting voltage plots were then used to determine the minimum energy needed to eject an electron from the sample surface. This minimum energy hereafter referred to as the photoemission threshold is defined by the midpoint between the onset binding energy and the binding energy of the secondary electron cutoff maximum (Figure SI3). An intensity at the higher electron kinetic energy at which the material no longer emits electrons is determined. This is assigned to the valence band maxima (VBM) for the samples.

Subtracting the energy of incident light from the Fermi energy level produces the relative value of the valence band maxima of the material. Pixel by pixel photoemission threshold and the valence band maxima for TiN as well as TiNCuPc samples on silicon substrate are presented in

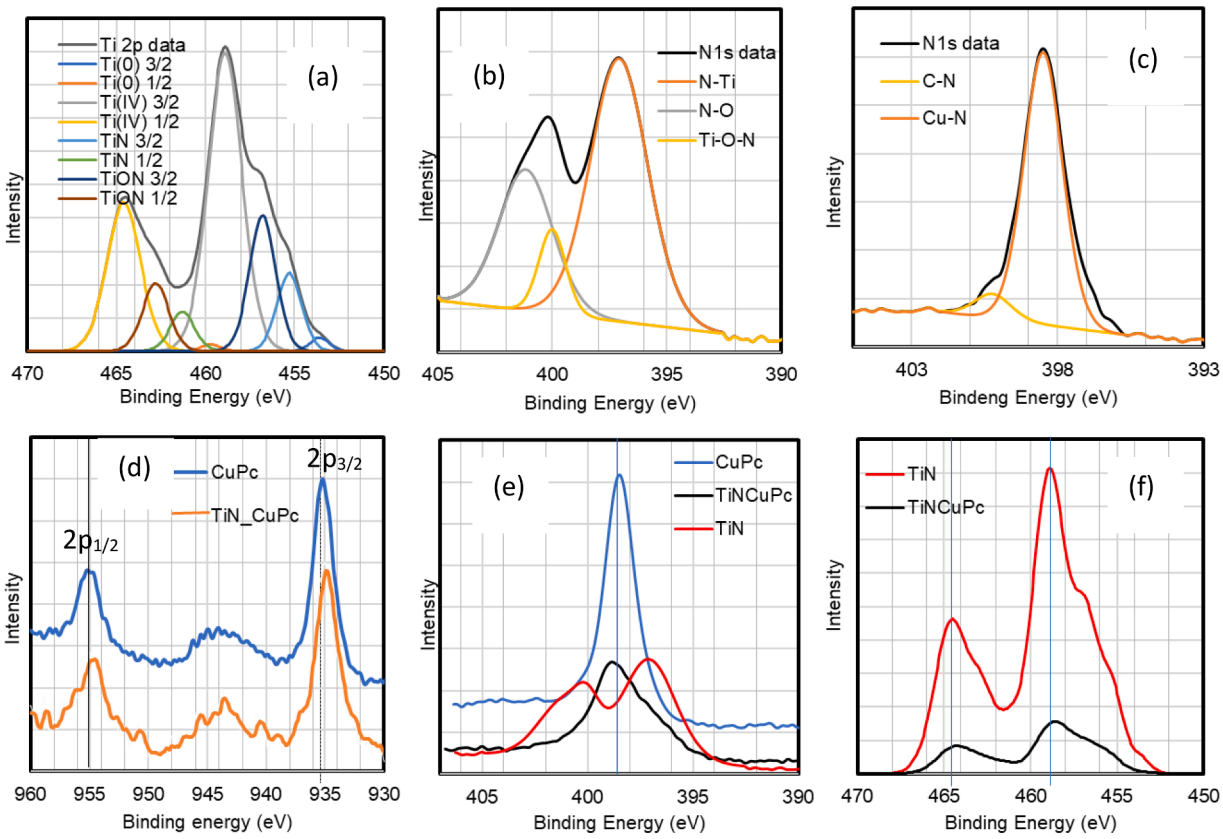

Fig. 3. (a) XPS Ti 2*p* Intensity of TiN peaks. (b) XPS N 1 s intensity of TiN (c) N 1 *s* peaks of CuPc (d) Cu 2*p* peaks comparison among CuPc and TiNCuPc (e) N 1 *s* peaks comparison among CuPc and TiNCuPc and TiN (f) Ti 2*p* peaks comparison among TiN and TiNCuPc. Color should be used for this figure.

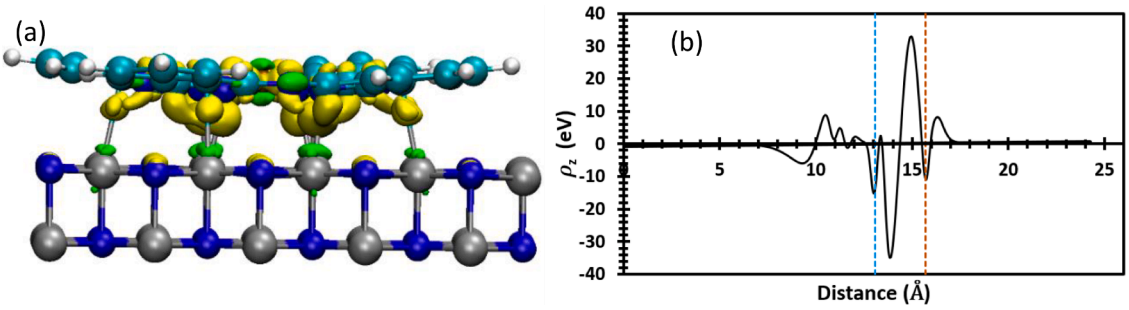

Fig. 4. (a) Charge Density difference for Pristine TiNCuPc. The yellow surface represents electron accumulation, and the lime green surface represents electron depletion with and isosurface values of 0.04 $e^-/Å^3$. The cyan, blue, grey, mauve, and white spheres represent C, N, Ti, Cu, and H, respectively. (b) Plane-averaged CDD along the surface normal direction of Pristine TiNCuPc (black solid line). The dashed blue line indicated the substrate charge and the orange dashed line indicates the charge of the Copper active site. Color should be used for this figure.

Fig. 5. The samples consist of regions with TiN or TiNCuPc deposited on silicon background, which appear as different image intensities (not shown here). The areas with lower photoemission intensity appear as yellow areas in Fig. 5 (a) and (c) are attributed to silicon background. The difference between the secondary electron cutoff and the valence band maxima represents the ionization potential for the material at that point. A histogram is constructed to determine the average ionization energies across the region of interest, which can be de-convoluted to determine the contribution from the silicon background as well as sample (Figure SI5). The ionization energies of silicon background can be used as a reference to determine the ionization energies of the samples. Since TiN exhibits metallic behavior, the VBM is essentially same as their Fermi energy level hence the ionization energy will be same as their work functions. The average work functions of TiN and TiNCuPC samples are shown in Fig. 6. The work function of TiNCuPc composites (4.34 eV) is lower than that of pure TiN (4.68 eV). This indicates it will be easier to withdraw electron from TiNCuPc composites with respect to TiN alone.

To corroborate the PEEM results, we have calculated the Ab Initio work function stem from non-bonded electronic potential in a vacuum with respect to the Fermi level energy expressed as $\varphi = V(\infty) - E_f$.[35] Fig. 6 shows experimentally measured as well as theoretically calculated work function values for different systems. PEEM measured work function for TiN is 4.68 eV which agrees well with other experimentally measured work functions for TiN reported in the literature.[36–38] However, the PEEM measured work function value for TiN nanoparticles is much higher than that of theoretically calculated work function of pristine stoichiometric TiN. The larger values of work functions observed in case of experimental measurements could be attributed to the unavoidable presence of surface oxide layer on TiN samples.

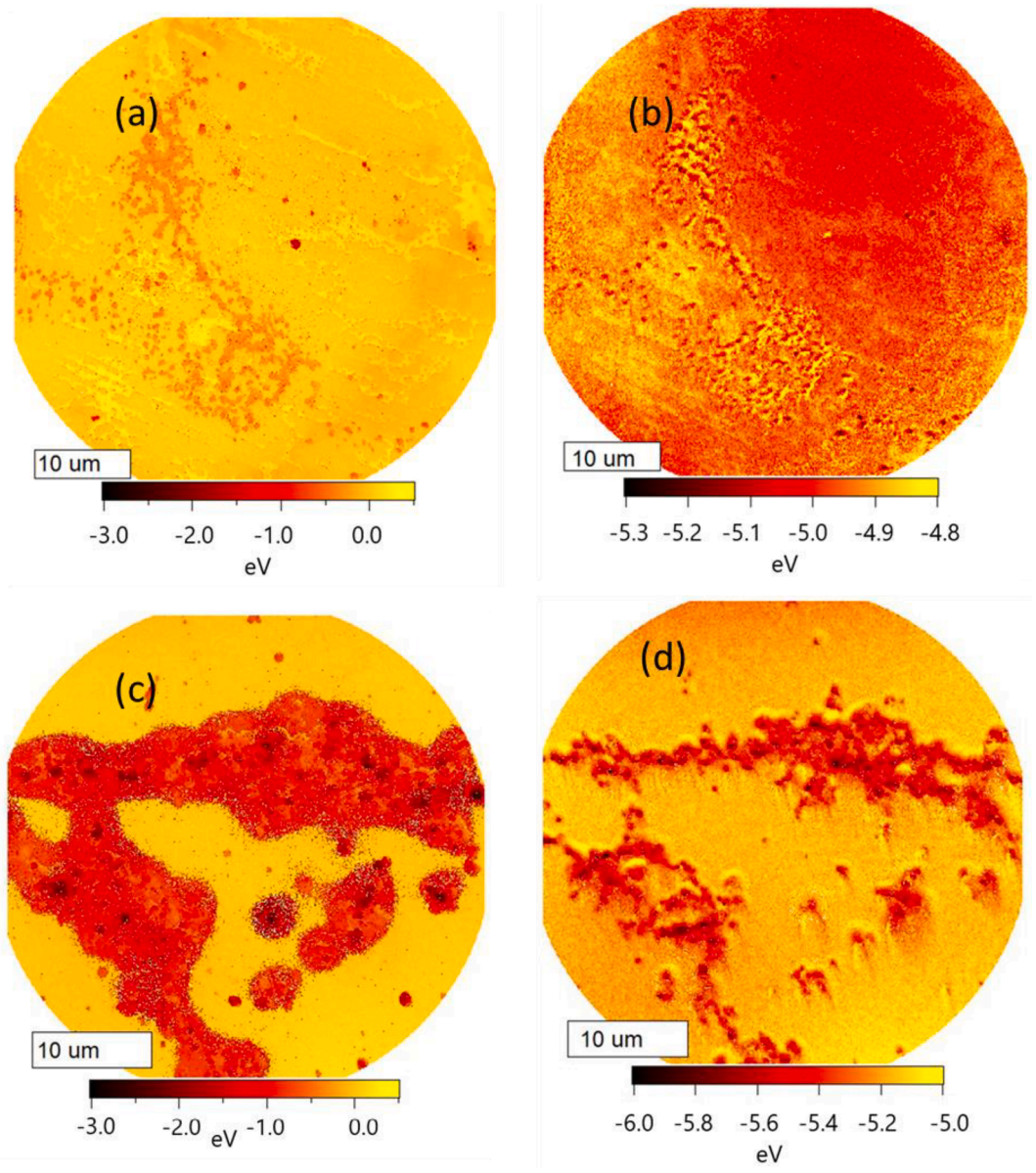

Fig. 5. (a) Photoemission threshold image for TiN on Si substrate. (b) VBM image of TiN on Si substrate. (c)Photoemission threshold image for TiN CuPc on Si substrate. (d) VBM image of TiN CuPc on Si substrate. The darker region in the images are assigned to TiN or TiNCuPc samples and the unform yellow background is assigned to silicon substrate. Color should be used for this figure.

Interestingly, there has been a study to increase work function of TiN by incorporating oxygen into it.[37] To further understand effect of oxygen on work functions, we also calculated the work function of TiN with oxide layer on top by replacing all the N atoms on the top layer by O atoms $(Ti_2NO)_{25}$ and the average work function was found to be about 2.98 eV, which is larger than the work function of pristine TiN as expected. The work function of the TiO_2 was also much larger than that of TiN. Our PEEM measured work function for TiN falls between pristine TiN and TiO_2 work functions, supports the presence of surface oxide layer on TiN.

4. Conclusions

We have studied the interaction among CuPc on TiN surfaces by means of X-ray photoelectron spectroscopy, Photoelectron emission Microscopy, and density functional theory-based calculations. Overall, we observe an excellent correlation between the experimental and theoretical results of the calculations and the experiments presented here. CuPc molecules bind strongly to the TiN surface indicating adsorption of CuPc on TiN substrate primarily through chemisorption. Both experimental and theoretical studies revealed a charge-transfer from the TiN substrate to the adsorbed CuPc molecule. PEEM measured work function of TiN agrees well with literature reported values. The work function of TiN is reduced due to the adsorption of CuPc on it. Interestingly, work function of pristine stoichiometric TiN obtained from Ab Initio based calculation is much lower than the PEEM measured work function of TiN nanoparticles, which could be due to the presence of few nm native oxide layer on the surface of TiN. This work provides a comprehensive understanding of electronic interaction among CuPc and TiN, which will open up new avenues in the field of catalysis as well as in optoelectronic devices.

Credit:

Philip Mantos: Conceptualization, Methodology, Software, Data curation, Writing- Original draft preparation. Chase Ferrone: Methodology, Software, Data curation, Writing- Original draft preparation. Sanchari Chowdhury: Conceptualization, Supervision, Methodology,

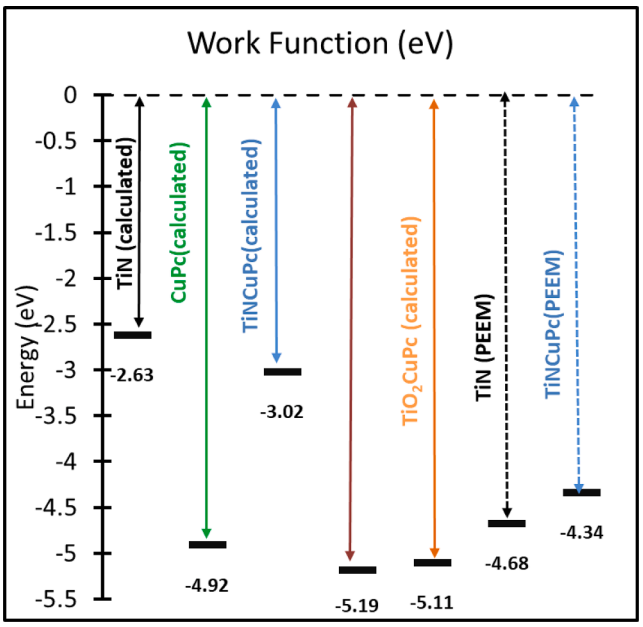

Fig. 6. Work functions (difference of vacuum level to valence band maximum) for different samples obtained from theoretical calculations as well as PEEM measurements. Color should be used for this figure.

Validation, Writing- Reviewing and Editing. Pabitra Choudhury: Supervision, Methodology, Writing- Reviewing and Editing. Taisuke Ohta: Supervision, Writing- Reviewing and Editing,

Funding Sources.

The work is supported by ACS-PRF Grant No [58740-UR6] and [60878 UR-6]. The PEEM work was supported by the Center for Integrated Nanotechnologies user program, an Office of Science User Facility operated for the U.S. Department of Energy (DOE) Office of Science (DE-AC04-94AL85000).

CRediT authorship contribution statement

Philip Mantos: Conceptualization, Methodology, Software, Data curation, Writing – original draft. **Chase Ferrone:** Methodology, Software, Data curation, Writing – original draft. **Taisuke Ohta:** Supervision, Writing – review & editing. **Pabitra Choudhury:** Supervision, Methodology, Writing – review & editing. **Sanchari Chowdhury:** Conceptualization, Supervision, Methodology, Validation, Writing – review & editing.

Declaration of Competing Interest

The authors declare that they have no known competing financial interests or personal relationships that could have appeared to influence the work reported in this paper.

Data availability

Data will be made available on request.

Acknowledgments

Acknowledgment is made to the Donors of the American Chemical Society Petroleum Research Fund for support (or partial support) of this research. The work is supported by ACS-PRF Grant No [58740-UR6] and [60878 UR-6], Authors also would like to thank NMT Chemical Engineering Scholarship for partial support. The PEEM work was supported by the Center for Integrated Nanotechnologies user program, an Office of Science User Facility operated for the U.S. Department of Energy (DOE) Office of Science (DE-AC04-94AL85000). This work used the Extreme Science and Engineering Discovery Environment (XSEDE) TACC at the stampede2 through allocation [TGDMR140131]. This work utilized resources from the University of Colorado Boulder Research Computing Group, which is supported by the National Science Foundation (awards ACI-1532235 and ACI-1532236), the University of Colorado Boulder, and Colorado. PCC Cluster, NM Consortium, NM.

Appendix A. Supplementary data

Supplementary data to this article can be found online at https://doi.org/10.1016/j.apsusc.2022.156204.

References

[1] L. Vijayan, A. Thomas, K.S. Kumar, K.B. Jinesh, Low power organic field effect transistors with copper phthalocyanine as active layer, J. Sci.: Adv. Mater. Devices 3 (3) (2018) 348–352.
[2] R. Jasinski, A new fuel cell cathode catalyst, Nature 201 (4925) (1964) 1212–1213.
[3] S. Roy, E. Reisner, Visible-Light-Driven CO2 Reduction by Mesoporous Carbon Nitride Modified with Polymeric Cobalt Phthalocyanine, Angewandte Chemie 131 (35) (2019) 12308–12312.
[4] M. Mukherjee, U.K. Ghorai, M. Samanta, A. Santra, G.P. Das, K.K. Chattopadhyay, Graphene wrapped Copper Phthalocyanine nanotube: Enhanced photocatalytic activity for industrial waste water treatment, Appl. Surf. Sci. 418 (2017) 156–162.
[5] D. Filonowich, M. Luna, T. Quinn, P. Choudhury, Electronic Descriptor of Single Metal-Oxo Species on Phthalocyanine- and Porphyrin-Functionalized Graphene toward Methane Activation Process, J. Phys. Chem. C 124 (8) (2020) 4502–4510.
[6] S. Yang, D.Y. Chung, Y.-J. Tak, J. Kim, H. Han, J.-S. Yu, A. Soon, Y.-E. Sung, H. Lee, Electronic structure modification of platinum on titanium nitride resulting in enhanced catalytic activity and durability for oxygen reduction and formic acid oxidation, Appl Catal B 174–175 (2015) 35–42.
[7] S. Yang, J. Kim, Y.J. Tak, A. Soon, H. Lee, Single-Atom Catalyst of Platinum Supported on Titanium Nitride for Selective Electrochemical Reactions, Angewandte Chemie International Edition 55 (6) (2016) 2058–2062.
[8] K.-G.-G.-C. De Silva, M. Finale, S. Chowdhury, Plasmon mediated deposition of Ni on titanium nitride nanoparticles: Applications in enhanced photoreduction of bicarbonate, Mater. Res. Bull. 152 (2022), 111834.
[9] S. Liu, W. Qi, S. Adimi, H. Guo, B. Weng, J.P. Attfield, M. Yang, Titanium Nitride-Supported Platinum with Metal-Support Interaction for Boosting Photocatalytic H2 Evolution of Indium Sulfide, ACS Appl. Mater. Interfaces 13 (6) (2021) 7238–7247.
[10] H. Nan, D. Dang, X.L. Tian, Structural engineering of robust titanium nitride as effective platinum support for the oxygen reduction reaction, J. Mater. Chem. A 6 (14) (2018) 6065–6073.
[11] D.C. Higgins, J.-Y. Choi, J. Wu, A. Lopez, Z. Chen, Titanium nitride–carbon nanotube core–shell composites as effective electrocatalyst supports for low temperature fuel cells, J. Mater. Chem. 22 (9) (2012) 3727–3732.
[12] Y. Dong, Y. Wu, M. Liu, J. Li, Electrocatalysis on Shape-Controlled Titanium Nitride Nanocrystals for the Oxygen Reduction Reaction, ChemSusChem 6 (10) (2013) 2016–2021.
[13] J. Zhang, H. Hu, X. Liu, D.S. Li, Development of the applications of titanium nitride in fuel cells, Mater. Today Chem. 11 (2019) 42–59.
[14] R.-Q. Zhang, T.-H. Lee, B.-D. Yu, C. Stampfl, A. Soon, The role of titanium nitride supports for single-atom platinum-based catalysts in fuel cell technology, PCCP 14 (48) (2012) 16552–16557.
[15] A. Catellani, P. D'Amico, A. Calzolari, Tailoring the plasmonic properties of metals: The case of substoichiometric titanium nitride, Physical Review Materials 4 (1) (2020), 015201.
[16] J.S.J. Hargreaves, Heterogeneous catalysis with metal nitrides, Coord. Chem. Rev. 257 (13) (2013) 2015–2031.
[17] J. Luo, H. Tang, X. Tian, S. Hou, X. Li, L. Du, S. Liao, Highly Selective TiN-Supported Highly Dispersed Pt Catalyst: Ultra Active toward Hydrogen Oxidation and Inactive toward Oxygen Reduction, ACS Appl. Mater. Interfaces 10 (4) (2018) 3530–3537.
[18] A. Beierle, P. Gieri, H. Pan, M.D. Heagy, A. Manjavacas, S. Chowdhury, Titanium nitride nanoparticles for the efficient photocatalysis of bicarbonate into formate, Sol. Energy Mater. Sol. Cells 200 (2019), 109967.
[19] P. Palmgren, K. Nilson, S. Yu, F. Hennies, T. Angot, J.M. Layet, G. Le Lay, M. Göthelid, Strong Interactions in Dye-Sensitized Interfaces, The Journal of Physical Chemistry C 112 (15) (2008) 5972–5977.
[20] P.A. Sharma, T. Ohta, M.T. Brumbach, J.D. Sugar, J. Michael, Ex Situ Photoelectron Emission Microscopy of Polycrystalline Bismuth and Antimony Telluride Surfaces Exposed to Ambient Oxidation, ACS Appl. Mater. Interfaces 13 (15) (2021) 18218–18226.
[21] G. Kresse, J. Furthmüller, Efficient iterative schemes for ab initio total-energy calculations using a plane-wave basis set, Phys. Rev. B 54 (16) (1996) 11169–11186.
[22] J.P. Perdew, K. Burke, M. Ernzerhof, Generalized Gradient Approximation Made Simple, Phys. Rev. Lett. 77 (18) (1996) 3865–3868.
[23] Perdew, J. P.; Burke, K.; Ernzerhof, M., Generalized Gradient Approximation Made Simple [Phys. Rev. Lett. 77, 3865 (1996)]. *Physical Review Letters* **1997,** *78* (7), 1396-1396.

[24] P.E. Blöchl, Projector augmented-wave method, Phys. Rev. B 50 (24) (1994) 17953–17979.
[25] G. Kresse, D. Joubert, From ultrasoft pseudopotentials to the projector augmented-wave method, Phys. Rev. B 59 (3) (1999) 1758–1775.
[26] G. Henkelman, A. Arnaldsson, H. Jónsson, A fast and robust algorithm for Bader decomposition of charge density, Comput. Mater. Sci 36 (3) (2006) 354–360.
[27] W. Tang, E. S., and G. Henkelman, A grid-based Bader analysis algorithm without lattice bias. *J. Phys.: Condens. Matter* **2009,** *21*, 084204.
[28] M. Yu, D.R. Trinkle, Accurate and efficient algorithm for Bader charge integration, J. Chem. Phys. 134 (6) (2011), 064111.
[29] B.W. Caplins, T.K. Mullenbach, R.J. Holmes, D.A. Blank, Femtosecond to nanosecond excited state dynamics of vapor deposited copper phthalocyanine thin films, PCCP 18 (16) (2016) 11454–11459.
[30] Ot E. Sielcken, M. M. v. T., Maarten F. M. Roks, Ron Hendriks,; Wiendelt Drenth, a. R. J. M. N., Synthesis and Aggregation Behavior of Hosts Containing Phthalocyanine and Crown Ether Subunits. *J. Am. Chem. Soc.* **1987,** *109*, 4261-426.
[31] A.C. Cruickshank, C.J. Dotzler, S. Din, S. Heutz, M.F. Toney, M.P. Ryan, The Crystalline Structure of Copper Phthalocyanine Films on ZnO(11¯00), J. Am. Chem. Soc. 134 (35) (2012) 14302–14305.
[32] N. Jiang, H.J. Zhang, S.N. Bao, Y.G. Shen, Z.F. Zhou, XPS study for reactively sputtered titanium nitride thin films deposited under different substrate bias, Physica B: Condensed Matter 352 (1) (2004) 118–126.
[33] N. Padma, S. Thomas, C.A. Betty, R. Rao, N. Gupta, K.G. Girija, Jagannath, Reversal of charge transfer direction at gold/copper phthalocyanine film interface on post deposition annealing: A vibrational spectroscopic study, Appl. Surf. Sci. 542 (2021), 148743.
[34] M. Berg, K. Keyshar, I. Bilgin, F. Liu, H. Yamaguchi, R. Vajtai, C. Chan, G. Gupta, S. Kar, P. Ajayan, T. Ohta, A.D. Mohite, Layer dependence of the electronic band alignment of few-layer $\mathrm{Mo}{\mathrm{S}}_{2}$ on $\mathrm{Si}{\mathrm{O}}_{2}$ measured using photoemission electron microscopy, Phys. Rev. B 95 (23) (2017), 235406.
[35] Seiji, K. T., N.; Jun, Y., Density Functional Calculation of Work Function Using Charged Slab Systems. *J. Phys.: Conf. Ser.* **2006,** *29*, 120.
[36] Filatova, E. O.; Konashuk, A. S.; Sakhonenkov, S. S.; Gaisin, A. U.; Kolomiiets, N. M.; Afanas'ev, V. V.; Dekkers, H. F. W., Mechanisms of TiN Effective Workfunction Tuning at Interfaces with HfO2 and SiO2. *The Journal of Physical Chemistry C* **2020,** *124* (28), 15547-15557.
[37] Z. Li, T. Schram, T. Witters, J. Tseng, S. De Gendt, K. De Meyer, Oxygen incorporation in TiN for metal gate work function tuning with a replacement gate integration approach, Microelectron. Eng. 87 (9) (2010) 1805–1807.
[38] Steven A. Vitale, J. K., Paul Healey, Peter W. Wyatt, and Craig L. Keast, Work-Function-Tuned TiN Metal Gate FDSOI Transistors for Subthreshold Operation. *IEEE Trans. Electron. Devices* **2011,** *58*.